RSC Advances

ROYAL SOCIETY OF CHEMISTRY

www.rsc.org/advances

Probing the structural and electronic properties of doped gallium oxide and sulfide, $M(GaX_2)_2$ where M = alkali or coinage metal; X = O, S

N. Seeburrun[a], I. A. Alswaidan[b], H.-K. Fun[b,c], E. F. Archibong[d], P. Ramasami[a,*]

[a]*Computational Chemistry Group, Department of Chemistry, Faculty of Science, University of Mauritius, Réduit, Mauritius*

[b]*Department of Pharmaceutical Chemistry, College of Pharmacy, King Saud University, P.O. Box 2457, Riyadh 11451, Saudi Arabia*

[c]*X-ray Crystallography Unit, School of Physics, Universiti Sains Malaysia, 11800 USM, Penang, Malaysia*

[d]*Department of Chemistry and Biochemsistry, University of Namibia, Namibia*

[*]Author for correspondence e-mail; p.ramasami@uom.ac.mu

Fax: +230 4656928

Tel: +230 4657507

Abstract

A theoretical study on the equilibrium geometries, vibrational frequencies and electronic features of a series of doped gallium oxide and sulfide, $M(GaX_2)_2$ (M = alkali or coinage metal; X = O or S), clusters was conducted. The ground and low-lying excited states of these clusters were studied using DFT, MP2 and single point CCSD(T) levels of theory, in conjunction with 6-311+G(2df) and Stuttgart quasi-relativistic pseudo-potential (SDD) basis sets. In most cases, the substitution of an alkali or a coinage metal atom in the gallium oxide and sulfide clusters does not affect drastically the structural characteristics. The vertical electron detachment energies (VEDEs) of gallium oxide and sulfide doped with alkali metals range from 2.88 [CCSD(T)//B3LYP)] to 4.51 (B3P86) eV while with the coinage metals, the values vary from 3.36 [CCSD(T)//MP2)] to 6.92 (MP2) eV. The VEDEs of coinage-gallium sulfide clusters namely $Cu(GaS_2)_2$, $Ag(GaS_2)_2$ and $Au(GaS_2)_2$ are higher than that of GaS_2. This feature is observed as the extra electron of the anions is localized mainly around the GaS_2 moiety. Further, anions with high VEDEs were interacted with a positive counter ion to form salts. The fragmentation energies indicate that the studied clusters are stable.

1. Introduction

Superhalogens have received substantial attention owing to their high electron affinities. Gutsev and Boldyrev proposed the general formula of a conventional superhalogen as $MX_{(n+1)/m}$ where M is a main group or transition metal atom with valency *n* and X is an electronegative atom with valency *m* [1,2]. Such species have electron affinities [1] above that of chlorine (3.62 eV) atom [3]. Superhalogens have immense potential in the field of synthesis of unusual organic compounds (e.g $Xe^{+}[PtF_6]^{-}$) [4]. Willis *et al*. [5] showed that hierarchical structures called "hyperhalogens" can be made by replacing halogen atoms in a traditional superhalogen with other superhalogens. Interestingly, the hyperhalogens should have electron affinities that even surpass their constituent superhalogen building blocks [5] and therefore can serve as ingredients in the synthesis of a new species known as 'hypersalt' [6].

Extensive efforts have been devoted over the past few years to the superhalogens [1,2,4,7–10]. Initially, a superhalogen consisted of a core metal atom surrounded by halogen atoms [1,2] but, it was found that clusters with no halogens or metal atoms or both could exhibit superhalogen properties [7–12]. For example, boron dioxide (BO_2) is a superhalogen even though it has a non-metal center surrounded by oxygen atoms [7]. Aluminium and gallium dioxide (AlO_2 and GaO_2) are superhalogens as their electron affinities exceed that of chlorine atom [8,9]. Turning to the sulfur congener, BS_2 [10] and GaS_2 [11] can act as superhalogens. The dimers M_2O_4 (M = B, Al and Ga) [8,9] can also be classified as superhalogens owing to their high electron affinities while B_2S_4 does not qualify to be a superhalogen [10]. Recently, Kandalam and co-workers [12] illustrated the ability of $(BO_2)_2$ and subsequent higher oligomers $(BO_2)_n$ (n = 3,4)

to retain their superhalogen characteristics. The interaction between Au atoms and BO_2 moieties [13] has been a driving force for the search of new hyperhalogens. The electron affinity of $Au(BO_2)_2$ is higher than that of BO_2 superhalogen and it is termed as a hyperhalogen [13]. A series of hyperhalogen species were studied experimentally and theoretically on simple metals (Zn [14] and Al [15]) and transition metal atoms containing boron oxide (Au [13,16,17], Cu [18], Ag [19,20], Mn and Fe [21]). Subsequent experiments were extended to $Al(BH_4)_n$, $Al(BF_4)_n$ (n = 1–4) [22], $Na[Na(BF_4)_2]_2$, $Li[Li(BF_4)_2]_2$ [23] and MAu_4 (M = Al and Ga) complexes [24] in order to confirm the hyperhalogen concept. Akin to BO_2 [7], BS_2 [10] is a potential hyperhalogen because the electron affinities of $Au(BS_2)_2$, $Li(BS_2)_2$ and $K(BS_2)_2$ surpass that of their building blocks BS_2.

In view of the above, the substitution of an atom by another can induce electronic properties. Fueled by these interesting results and an urge to see if significant differences in the properties are noted on going from boron to gallium and oxygen to sulfur, the objectives of this investigation were: (i) to study the equilibrium structures of dimeric GaO_2 and GaS_2 doped with alkali (Li, Na and K) and coinage (Cu, Ag and Au) metals (ii) to provide a reliable theoretical prediction of the relative stabilities, harmonic vibrational frequencies and energetic features (iii) to compare the ground state geometries with analogous boron and aluminium structures and finally (iv) to determine whether the studied clusters possess electron affinities higher than those of building blocks.

2. Computational details

Electronic structure computations of neutral and negatively charged $M(GaX_2)_2$ [M is an alkali metal (Li, Na and K) or a coinage metal (Cu, Ag and Au) and X is O or S] were performed using Gaussian 09 [25] program package by means of the resources provided by GridChem Science Gateway [26–28]. Initial configurations considered for geometry optimizations were taken from previous investigations on valence isoelectronic boron oxide [7] and sulfide [10]. New initial structures with superhalogen moieties bound to the metal atom were also considered to determine the ground state geometries. The tight convergence criterion was applied for all the computations. The 6-311+G(2df) one-particle basis set was employed for Li, Na, K, Ga, O and S [9,11] atoms and the Stuttgart quasi-relativistic pseudo-potential (SDD) basis set was used for Cu, Ag and Au atoms [29–31]. The density functional theory (DFT) with the B3P86, B3PW91 and B3LYP functionals [32–37] and the MP2 [38,39] method were employed. To calculate the electronic properties of the ground state geometries, single point computations at the CCSD(T) level [40] were performed by using B3LYP and MP2 optimized structures. The adiabatic electron affinity (AEA), adiabatic electron detachment energy (AEDE) and vertical electron detachment energy (VEDE) were calculated as follows:

AEA = *E* (optimized neutral at ground state) − *E* (optimized anion at ground state);

AEDE = *E* (optimized corresponding neutral) − *E* (optimized anion);

VEDE = *E* (neutral at optimized anion geometry) − *E* (optimized anion).

Furthermore, the harmonic vibrational frequencies of the optimized geometries were also analyzed to verify the nature of the stationary points. Natural bond orbital (NBO) analysis

[41,42] was performed theoretically to provide an insight into the bonding nature of the studied species. The HOMO−LUMO (H−L) gaps of the studied clusters were calculated with the B3LYP functional.

3. Results and discussion

Optimized geometrical configurations of the lowest-lying energy states of the studied clusters are shown in Figs. 1–4 while the low-lying structures are presented in Figs. S1 and S2. The relative energies (ΔE) of the ground state geometries and first low-lying isomers are listed in Tables 1 and 2. The internal coordinates of the ground state geometries and harmonic vibrational computations are available in the Supporting Information section (Tables S1–S6). The AEAs, AEDEs and VEDEs of the studied clusters using different levels of theory are presented in Table 3.

3.1 Structural and Geometrical Properties

The ground state geometry of neutral and anionic $Li(GaO_2)_2$ is composed of a dimerized GaO_2 bound to a Li atom, which is of C_s symmetry (Fig. 1). Similar lowest-energy configuration was observed for doped sodium aluminium oxide congener [8]. The substitution of a Li atom by Na and K atoms does not alter the structural properties of alkali-gallium oxide clusters. Akin to $Li(GaO_2)_2$, neutral and anionic $Na(GaO_2)_2$ and $K(GaO_2)_2$ consist of a dimerized GaO_2 bound to their corresponding alkali metals (Fig. 1). Analogous with neutral $Li(BS_2)_2$ [10], $Li(GaS_2)_2$ consists of a dimerized GaS_2 in which the Li atom is attached to one sulfur atom (C_1 symmetry) (Fig. 2). Anionic $Li(GaS_2)_2$ adopts the same ground state geometry as the oxygen analogue.

Neutral $Li(GaO_2)_2$ and $Li(GaS_2)_2$ maintain the geometries of their corresponding dimers [9,11]. Neutral and anionic $Na(GaS_2)_2$ adopt same ground state geometries as neutral and anionic $Li(GaS_2)_2$. On the other hand, neutral and anionic $K(GaS_2)_2$ possess similar ground state geometries as the oxygen congener. The terminal Ga–X bond remains fairly constant while the Ga–X–M (M = Li, Na and K; X = O and S) bond angle increases from lithium to potassium series in the neutral and anionic doped gallium oxide and sulfide clusters. The increase in bond angle can be explained by the increase in size from lithium to potassium atom. A decrease in the terminal bond length and Ga–X–M (M = Li, Na and K; X = O and S) bond angle is observed from the neutral to its corresponding anion. The low-lying isomer of neutral $Li(GaO_2)_2$ is formed by the rupture of one Li–O bond, thus leading to a structure which is composed of a Li atom attached linearly to the planar 'D_{2h}' geometry of Ga_2O_4 while that of its anion is linear. The low-lying configuration of $Li(GaS_2)_2$ resembles the ground state geometry but is of C_s symmetry. The isomer is, 0.003 eV (Table 1) above the ground state geometry with the three DFT functionals. Akin to neutral $Li(GaO_2)_2$, the low-lying configuration of neutral and anionic $M(GaO_2)_2$ (M = Na and K) and neutral $M(GaS_2)_2$ (M = Na and K) is composed of the alkali metal atom attached linearly to the planar 'D_{2h}' geometry of Ga_2O_4/Ga_2S_4. A planar chair-like structure (C_{2h} symmetry) is obtained as the low-lying isomer for anionic $M(GaS_2)_2$ (M = Li, Na and K) (Fig. S1).

Turning to the coinage metals, neutral $Cu(GaO_2)_2$ is composed of a Cu atom attached diagonally to one terminal oxygen atom of the planar 'D_{2h}' geometry of Ga_2O_4 (C_s symmetry) (Fig. 3). The anion adopts a twisted chair-like structure (C_{2h} symmetry) with each GaO_2 unit attached to the Cu atom unlike analogous $Cu(BO_2)_2$ which is planar [19]. Neutral $Ag(GaO_2)_2$ and $Au(GaO_2)_2$

possess the same ground state geometry as $Cu(GaO_2)_2$. The lowest-energy configuration of anionic $Ag(GaO_2)_2$ adopts a structure similar to anionic $M(GaO_2)_2$ (M = Li, Na and K) while that of anionic $Au(GaO_2)_2$ resembles the copper congener and $Au(BO_2)_2$ [19]. The M–O–Ga (M = Cu, Ag and Au) bond angle increases in the order $Cu(GaO_2)_2 > Ag(GaO_2)_2 > Au(GaO_2)_2$. However, the terminal Ga–O bond length increases in the order $Ag(GaO_2)_2 > Au(GaO_2)_2 > Au(GaO_2)_2$. A similar geometric trend was reported with the coinage-boron oxide clusters [19]. Neutral $Cu(GaS_2)_2$ is composed of a pentagon to which a sulfur atom is bound to one gallium atom and the other gallium atom forms a cyclic moiety with the copper and sulfur atoms (Fig. 4). Anionic $Cu(GaS_2)_2$ adopts a distorted chair-like configuration. Akin to the oxide analogue, $Ag(GaS_2)_2$ comprises of a Ag atom attached diagonally to one terminal sulfur atom of the planar 'D_{2h}' geometry of Ga_2S_4. Neutral $Au(GaS_2)_2$ adopts the same structure as $Cu(GaS_2)_2$. Anionic $Ag(GaS_2)_2$ and $Au(GaS_2)_2$ adopt planar chair-like structures. It is noteworthy that $Ag(BO_2)_2^-$ and $Au(BO_2)_2^-$ [19] possess similar but non-planar geometries. The geometry of GaS_2^- is almost unchanged in the case of anionic $M(GaS_2)_2$ (M = Cu, Ag and Au), indicating its integrity in bonding with the central metal atoms. Similarly, the Ga–S bond length of the GaS_2 moiety remains fairly constant but the M–S–Ga bond angle of $Ag(GaS_2)_2$ is largest followed by $Cu(GaS_2)_2$. The low-lying isomer of neutral $Cu(GaO_2)_2$ is similar to the ground state geometry of $M(GaO_2)_2$ (M = Li, Na and K) and that of $Cu(GaS_2)_2$ resembles its ground state geometry but with the cyclic moiety arranged in a distorted manner (Fig. S2). In the case of $Ag(GaO_2)_2$, the low-lying isomer is composed of a silver metal atom attached linearly to the planar 'D_{2h}' geometry of Ga_2O_4 while for $Au(GaO_2)_2$ and $Au(GaS_2)_2$, the gold atom is attached diagonally. The low-lying configuration of $Ag(GaS_2)_2$ is above the ground state geometry with energies of 0.02 (B3PW91 and B3LYP) and 0.42 eV (MP2) (Table 2), respectively. Anionic $Cu(GaO_2)_2$,

$Au(GaO_2)_2$ and $Cu(GaS_2)_2$ prefer planar chair-like configurations and anionic $Ag(GaO_2)_2$, $Ag(GaS_2)_2$ and $Au(GaS_2)_2$ adopt W-shaped geometries as first low-lying isomers.

3.2 Vibrational Properties

The harmonic vibrational frequencies of the lowest-energy states of the clusters are presented in Tables S1–S6 (Supporting Information). All the ground state geometries of the studied doped gallium oxide and sulfide clusters do not have imaginary vibrational frequencies with the B3LYP functional and MP2 method. An analysis of the modes of vibration of $M(GaX_2)_2$ (M = Li, Na and K; X = O and S) indicates that the highest frequency mode corresponds to the asymmetrical Ga–X stretch which is bound to the rhombic Ga_2X_2 and alkali metal. In the case of anionic $M(GaX_2)_2$, with the exception of anionic $Li(GaS_2)_2$, the highest frequency mode is attributed to the stretching of the terminal Ga–X bond. The most active mode of $Cu(GaO_2)_2$, $Ag(GaO_2)_2$ and $Au(GaO_2)_2$ is the stretching of the Ga–O bond attached to the corresponding coinage metal while that of $Ag(GaS_2)_2$ refers to the symmetrical stretching of the Ga_2S_2 ring. The highest frequencies of $Cu(GaS_2)_2$ and $Au(GaS_2)_2$ correspond to the stretching of the Ga–S bond in the cyclic moiety. For anionic $Cu(GaO_2)_2$, $Au(GaO_2)_2$, $Cu(GaS_2)_2$, $Ag(GaS_2)_2$ and $Au(GaS_2)_2$, the stretching along the linear GaO_2/GaS_2 moiety has the highest frequency value while that of anionic $Ag(GaS_2)_2$ corresponds to the terminal Ga–S stretch.

3.3 Electronic Properties

I. AEAs, AEDEs and VEDEs

As the ground state structures of neutral and anionic $M(GaO_2)_2$ (M = Li, Na and K) and $K(GaS_2)_2$ are identical, the AEDEs of the anionic clusters correspond to the AEAs of the neutral clusters (Table 3). The AEAs of the studied clusters at the CCSD(T)//B3LYP and CCSD(T)//MP2 levels are collected in Table S7. The AEAs of $Li(GaO_2)_2$ are 3.98 (B3P86), 3.37 (B3PW91), 3.46 (B3LYP), 3.82 (MP2) and 3.40 eV with the single point CCSD(T) computations. The AEA of $Li(GaO_2)_2$ is less than that of the GaO_2 superhalogen at the DFT, MP2 and CCSD(T)//B3LYP and CCSD(T)//MP2 levels and is even smaller when compared to dimeric GaO_2 superhalogen [9]. The AEAs of $Li(GaS_2)_2$ are 4.24 (B3P86), 3.67 (B3PW91), 3.69 (B3LYP), 3.72 (MP2), 3.51 [CCSD(T)//B3LYP] and 3.59 [CCSD(T)//MP2] eV. The AEA value of $Li(GaS_2)_2$ surpass that of GaS_2 with the B3P86 functional only. The question that arises is: can $Li(GaS_2)_2$ be classified as a hyperhalogen when its AEA is higher than that of GaS_2? To solve this ambiguity, the VEDEs of the anions were calculated (Table 3). The VEDEs of $Li(GaS_2)_2$ are higher in comparison to that of GaS_2 at the B3P86, B3LYP and MP2 levels. Consequently, the possibility of $Li(GaS_2)_2$ behaving as a hyperhalogen is negated. Turning to the sodium and potassium series, $Na(GaO_2)_2$ and $K(GaO_2)_2$ and their respective sulfur analogues possess smaller AEA values than GaO_2 and GaS_2 at different levels of theory employed. Again, these clusters cannot be classified as hyperhalogens.

The AEAs of coinage-gallium oxide (M = Cu, Ag and Au) clusters are lower than the GaO_2 superhalogen at all the levels of theory employed and therefore cannot be classified as hyperhalogens. However, they have substantially high VEDE values. For instance, $Au(GaO_2)_2$

has the highest VEDE among the oxide series. Akin to the boron congener [19], $Ag(GaO_2)_2$ has higher VEDE values than $Au(GaO_2)_2$. $Cu(GaS_2)_2$, $Ag(GaS_2)_2$ and $Au(GaS_2)_2$ display high VEDE values at different levels of theory employed, with $CuGa_2S_4$ having a VEDE of 6.92 eV (MP2). However, the AEAs of $Cu(GaS_2)_2$, $Ag(GaS_2)_2$ and $Au(GaS_2)_2$ are higher than that of GaS_2 with the B3P86 functional only. Therefore, the possibility of such clusters to exist as 'hyperhalogen' is negated.

II. NBO charges

In order to analyze the distribution of the extra charge in the anionic species, the NBO [41,42] charges on the alkali and coinage metals of each cluster are summarized in Table 4 and the contribution of the atoms to the selected orbitals are given in Tables S8–11. The charges on alkali and coinage metal atoms are positive. The excess electron in the anionic gallium oxide doped with alkali metals is mainly localized on the oxygen atom of the terminal Ga–O bond from the charge density plots (Fig. S3). This is further confirmed by natural population analysis (NPA). The bonding orbital on the Ga−O terminal bond has more contribution from the oxygen atoms (Table S8). Akin to the oxygen analogue, the excess electron in the anionic gallium sulfide doped with alkali metals is localized on the sulfur atom of the terminal Ga–S bond (Fig. S3). Turning to the coinage metal, the excess electron is delocalised over the OCuO moiety for $Cu(GaO_2)_2^-$, terminal Ga–O bond for $Ag(GaO_2)_2^-$ and over the whole system for $Au(GaO_2)_2^-$. The excess electron in the anionic gallium sulfide doped with coinage metals is localized on the sulfur atoms (Fig. 4).

III. HOMO–LUMO gaps

The HOMO–LUMO gaps of the neutral clusters are presented in Table 5. A large value of the HOMO–LUMO energy gap enhances the chemical stability of the cluster [43]. The HOMO–LUMO gaps of the lowest-energy configurations are large, varying from 3.33 [$Ag(GaS_2)_2$] to 5.04 eV [$Li(GaO_2)_2$] with the B3LYP functional. A decrease in the HOMO–LUMO gaps is observed from $Li(GaO_2)_2$ to $K(GaO_2)_2$ and from $Li(GaS_2)_2$ to $K(GaS_2)_2$. This feature can be rationalized by the size of atom. Similar decrease in the HOMO–LUMO gaps is seen from $Cu(GaO_2)_2$ to $Au(GaO_2)_2$ but an irregular trend is noted for the sulfur counterpart.

IV. Thermodynamic Stability

The thermodynamic stabilities of the lowest-energy isomers for neutral clusters were examined against fragmentation into selected channels (Table 6). The dissociation energy (D_e) is obtained as the difference in total energies of the initial state and the sum of total energies of the decay fragments. The ground state geometries of neutral $MGaX_2$ (M = alkali or coinage metal; X = O or S) was explored in order to determine the dissociation energies of $M(GaX_2)_2$. The dissociation energies are all positive, indicating these clusters are stable against any fragmentation. The $M(GaX_2)_2 \rightarrow M(GaX_2) + GaX_2$ (M = Li, Na and K; X = O, S) fragmentation pathway requires lower energies than the $M(GaX_2)_2 \rightarrow M + (GaX_2)_2$ process. Similar feature is observed for gallium sulfide doped with copper and silver metals. However, the most preferred channel of the oxide series is $M(GaO_2)_2 \rightarrow M + (GaO_2)_2$ (M = Cu, Ag and Au). No significant trend is observed on the dissociation energy values upon substitution of the alkali or coinage metal atom to the gallium oxide and sulfide clusters.

V. Interaction with electropositive potassium counter ion

Although $Cu(GaS_2)_2$, $Ag(GaS_2)_2$ and $Au(GaS_2)_2$ cannot be classified as hyperhalogens, these clusters were interacted with a countercation. This was done by adding a positive ion such as K^+ to the anionic ground state geometries. Fig. 5 shows the ground state structures of these salt moieties. The stability of these salts was determined by considering the energetics of the following fragmentation pathways [6]:

$\Delta E_1 = -[KMGa_2X_4 - K^+ - MGa_2X_4^-]$

$\Delta E_2 = -[KMGa_2X_4 - K - MGa_2X_4]$

$\Delta E_3 = -[KMGa_2X_4 - KGaX_2 - MGaX_2]$

These energies, given in Table 7, are positive, indicating that the salts' clusters are stable with respect to fragmentation.

4. Conclusions

Using DFT, MP2 and single point CCSD(T) based computations, a systematic theoretical study of the structures and stabilities of neutral and anionic $M(GaX_2)_2$ (M = alkali or coinage metal; X = O or S) was carried out. The substitution of a Li atom by Na and K in the studied gallium oxide and sulfide clusters does not alter the structural properties. The AEAs and VEDEs of $M(GaX_2)_2$ (M = alkali metal; X = O or S) are lower than that of GaO_2 and GaS_2, respectively. On the other hand, the VEDEs of gallium oxide and sulfide containing coinage metals are substantially higher but with AEAs lower than the ones for GaO_2 and GaS_2. On this basis, none of the studied clusters can be termed as hyperhalogens. Because experimental data are limited,

these results open more ventures on future experimental and theoretical studies regarding doped gallium oxide and sulfide clusters.

5. References

1. G. L. Gutsev and A. I. Boldyrev, *Chem. Phys*., 1981, **56**, 277.
2. G. L. Gutsev and A. I. Boldyrev, *Adv. Chem. Phys*., 1985, **61**, 169.
3. H. Hotop and W. C. Lineberger, *J. Phys. Chem. Ref. Data*, 1985, **14**, 731.
4. N. Bartlett, *Proc. Chem. Soc. (London)* 1962, **6**, 218.
5. M. Willis, M. Götz, A. K. Kandalam, G. F. Ganteför and P. Jena, *Angew. Chem*., 2010, **122**, 9150.
6. S. Behera, D. Samanta and P. Jena, *J. Phys. Chem. A*, 2013, **117**, 5428.
7. H. Zhai, L. Wang, S. Li and L. Wang, L. *J. Phys. Chem. A* 2007, **111**, 1030.
8. K. Pradhan and P. Jena, *J. Chem. Phys.*, 2011, **135**, 144305.
9. N. Seeburrun, H. H. Abdallah and P. Ramasami, *J. Phys. Chem. A*, 2012, **116**, 3215.
10. L.-P. Ding, X.-Y. Kuang, S. Shao, M.-M. Zhong and Y.-R. Zhao, *RSC Adv*., 2013, **3**, 15449.
11. N. Seeburrun, H. H. Abdallah, E. F. Archibong and P. Ramasami, *Struc. Chem.*, 2014, **25**, 755.
12. A. K. Kandalam, K. Boggavarappu, P. Jena, S. Pietsch and G. Ganteför, *Phys. Chem. Chem. Phys.*, 2015, **17**, 26589.
13. M. Willis, M. Götz, A. K. Kandalam, G. F. Ganteför and P. Jena, *Angew. Chem. Int. Ed.* 2010, **49**, 8966.
14. D. Samanta, M. M. Wu and P. Jena, *J. Am. Chem. Soc*., 2012, **134**, 8400.

15. G. L. Gutsev, C. A. Weatherford, L. E. Johnson and P. Jena, *J. Comput. Chem*., 2012, **33**, 416.

16. M. Götz, M. Willis, A. K. Kandalam, G. F. Ganteför and P. Jena, *Chem. Phys. Chem*., 2010, **11**, 853.

17. W.-J Tian, H.-G Xu, X.-Y Kong, Q. Chen, W.-J Zheng, H.-J Zhai and S.-D Li, *Phys. Chem. Chem. Phys.*, 2014, **16**, 5129.

18. Y. Feng, H.-G. Xu, W. J. Zheng, H. M. Zhao, A. K. Kandalam and P. Jena, *J. Chem. Phys*., 2011, **134**, 094309.

19. H. Chen, X.-Y. Kong, W. Zheng, J. Yao, A. K. Kandalam and P. Jena, *Chem. Phys. Chem*., 2013, **14**, 3303.

20. X.-Y Kong, H.-G Xu, P. Koirala, W.-J Zheng, A. K. Kandalam and P. Jena, *Phys. Chem. Chem. Phys.*, 2014, **16**, 26067.

21. P. Koirala, K. Pradhan, A. K. Kandalam and P. Jena, *J. Phys. Chem. A* 2013, **117**, 1310.

22. C. Paduani, M. M. Wu, M. Willis and P. Jena, *J. Phys. Chem. A*, 2011, **115**, 10237.

23. C. Paduani and P. Jena, *J. Phys. Chem. A*, 2012, **116**, 1469.

24. T. Zhao, Y. Li, Q. Wang and P. Jena, *Chem. Phys. Chem*., 2013, **14**, 3227.

25. Gaussian 09, Revision D.01, M. J. Frisch, G. W. Trucks, H. B. Schlegel, G. E. Scuseria, M. A. Robb, J. R. Cheeseman, G. Scalmani, V. Barone, B. Mennucci, G. A. Petersson, H. Nakatsuji, M. Caricato, X. Li, H. P. Hratchian, A. F. Izmaylov, J. Bloino, G. Zheng, J. L. Sonnenberg, M. Hada, M. Ehara, K. Toyota, R. Fukuda, J. Hasegawa, M. Ishida, T. Nakajima, Y. Honda, O. Kitao, H. Nakai, T. Vreven, J. A. Montgomery, Jr., J. E. Peralta, F. Ogliaro, M. Bearpark, J. J. Heyd, E. Brothers, K. N. Kudin, V. N. Staroverov, R. Kobayashi, J. Normand, K. Raghavachari, A. Rendell, J. C. Burant, S. S. Iyengar, J. Tomasi, M. Cossi,

N. Rega, J. M. Millam, M. Klene, J. E. Knox, J. B. Cross, V. Bakken, C. Adamo, J. Jaramillo, R. Gomperts, R. E. Stratmann, O. Yazyev, A. J. Austin, R. Cammi, C. Pomelli, J. W. Ochterski, R. L. Martin, K. Morokuma, V. G. Zakrzewski, G. A. Voth, P. Salvador, J. J. Dannenberg, S. Dapprich, A. D. Daniels, Ö. Farkas, J. B. Foresman, J. V. Ortiz, J. Cioslowski, and D. J. Fox, Gaussian, Inc., Wallingford CT, 2009.

26. R. Dooley, K. Milfeld, C. Guiang, S. Pamidighantam and G. J. Allen, *J. Grid Comput.*, 2006, **4**, 195.
27. K. Milfeld, C. Guiang, S. Pamidighantam and J. Giuliani, *Proceedings of the 2005 Linux Clusters: The HPC Revolution Linux Clusters Institute*, 2005.
28. R. Dooley, G. Allen and S. Pamidighantam, *Proceedings of the 13th Annual Mardi Gras Conference Louisana State University, Baton Rouge, LA*, 2005.
29. P. Schwerdtfeger, M. Dolg, W. H. E. Schwarz, G. A. Bowmaker and P. D. W. Boyd, *J. Chem. Phys.*, 1989, **91**, 1762.
30. M. Dolg, U. Wedig, H. Stoll and H. Preuss, *J. Chem. Phys*., 1987, **86**, 866.
31. P. Koirala, M. Willis, K. Boggavarapu, A. K. Kandalam and P. Jena, *J. Phys. Chem. C*, 2010, **114**, 16018.
32. J. P. Perdew, *Phys. Rev. B*, 1986, **33**, 8822.
33. J. P. Perdew, *Phys. Rev. B*, 1986, **34**, 7406.
34. J. P. Perdew and Y. Wang, *Phys. Rev. B*, 1992, **45**, 13244.
35. J. P. Perdew, J. A. Chevary, S. H. Vosko, K. A. Jackson, M. R. Pederson, D. J. Singh and C. Fiolhais, *Phys. Rev. B*, 1992, **46**, 6671.
36. C. Lee, W. Yang and R. G. Parr, *Phys. Rev. B*, 1988, **37**, 785.
37. A. D. Becke, *J. Chem. Phys*., 1993, **98**, 5648.

38. R. J. Bartlett, *Ann. Rev. Phys. Chem*., 1981, **32**, 359.

39. W. J. Hehre, L. Radom, P. v. R. Schleyer and J. A. Pople, *Ab Initio Molecular Orbital Theory*; Wiley: New York, 1986.

40. K. Raghavachari, K, G. W. Trucks, J. A. Pople, M. Head-Gordon, M. *Chem. Phys. Lett*., 1989, **157**, 479.

41. A. E. Reed, L. A. Curtiss and F. Weinhold, *Chem. Rev*., 1988, **88**, 899.

42. A. E. Reed, R. B. Weinstock and F. Weinhold, *J. Chem. Phys*., 1985, **83**, 735.

43. M. M. Zhong, X. Y. Kuang, Z. H. Wang, P. Shao and L. P. Ding, *J. Mol. Model*., 2013, **19**, 263.

Acknowledgments

N.S. acknowledges support from the Mauritius Tertiary Education Commission (TEC) for the grant of MPhil/PhD scholarship. The authors also acknowledge facilities from the University of Mauritius and University of Namibia. The authors extend their appreciation to the Deanship of Scientific Research at King Saud University for the research group Project No. RGP VPP-207.

Supporting Information

Tables containing internal coordinates of the ground state geometries, harmonic vibrational wavenumbers (cm^{-1}) and total energies (Hartree) of the studied clusters. Figures of low-lying isomers and HOMOs of excess electron of anionic $M(GaX_2)_2$ (M = alkali or coinage metal; X = O and S).

List of Tables

Table 1: Energy shifts (eV) of the first low-lying isomers with respect to ground state geometries of $M(GaX_2)_2$ clusters where M = alkali metal; X = O, S

Cluster	**B3P86**	**B3PW91**	**B3LYP**	**MP2**
$Li(GaO_2)_2$	0.08	0.08	0.07	0.11
$Li(GaO_2)_2^-$	0.94	0.86	0.66	0.99
$Na(GaO_2)_2$	0.18	0.17	0.18	0.19
$Na(GaO_2)_2^-$	0.90	0.88	0.88	0.89
$K(GaO_2)_2$	0.09	0.08	0.08	0.14
$K(GaO_2)_2^-$	0.71	0.69	0.69	1.07
$Li(GaS_2)_2$	0.003	0.003	0.003	0.0006
$Li(GaS_2)_2^-$	0.78	0.73	0.46	0.98
$Na(GaS_2)_2$	0.53	0.53	0.53	0.54
$Na(GaS_2)_2^-$	0.72	0.66	0.41	1.07
$K(GaS_2)_2$	0.40	0.39	0.39	0.44
$K(GaS_2)_2^-$	0.78	0.71	0.47	1.72

Table 2: Energy shifts (eV) of the first low-lying isomers with respect to ground state geometries of $M(GaX_2)_2$ clusters where M = coinage metal; X = O, S

Cluster	**B3P86**	**B3PW91**	**B3LYP**	**MP2**
$Cu(GaO_2)_2$	0.04	0.08	0.11	0.16
$Cu(GaO_2)_2^-$	0.0009	0.001	–0.0001	0.03
$Ag(GaO_2)_2$	0.22	0.21	0.20	0.16
$Ag(GaO_2)_2^-$	0.61	0.56	0.42	0.80
$Au(GaO_2)_2$	0.40	0.60	0.62	0.36
$Au(GaO_2)_2^-$	0.02	0.02	0.02	0.05
$Cu(GaS_2)_2$	0.20	0.18	0.26	0.29
$Cu(GaS_2)_2^-$	0.005	0.005	0.003	0.03
$Ag(GaS_2)_2$	–0.02	0.02	0.02	0.42
$Ag(GaS_2)_2^-$	0.07	0.07	0.06	0.08
$Au(GaS_2)_2$	0.37	0.32	0.25	0.53
$Au(GaS_2)_2^-$	0.11	0.11	0.08	0.18

Table 3: Adiabatic electron affinities (AEAs), adiabatic electron detachment energies (AEDEs) and vertical electron detachment energies (VEDEs) of the studied clusters using different levels of theory

Methods	**B3P86**			**B3PW91**			**B3LYP**			**MP2**		
	AEA	**AEDE**	**VEDE**	**AEA**	**AEDE**	**VEDE**	**AEA**	**AEDE**	**VEDE**	**AEA**	**AEDE**	**VEDE**
$Li(GaO_2)_2$	3.98	3.98	4.33	3.37	3.37	3.73	3.46	3.46	3.81	3.82	3.82	4.19
$Na(GaO_2)_2$	3.71	3.71	4.02	3.01	3.01	3.42	3.20	3.20	3.50	3.54	3.54	3.91
$K(GaO_2)_2$	3.56	3.56	3.87	2.95	2.95	3.26	3.03	3.03	3.33	3.44	3.44	4.02
$Cu(GaO_2)_2$	3.92	5.15	4.83	3.31	4.55	5.42	3.53	4.58	4.86	4.05	4.02	6.07
$Ag(GaO_2)_2$	3.97	3.99	4.29	3.33	3.37	3.68	3.39	3.39	3.75	3.76	3.74	5.70
$Au(GaO_2)_2$	3.89	5.65	5.84	3.28	5.06	5.24	3.43	5.07	5.25	3.86	5.37	6.10
$Li(GaS_2)_2$	4.24	4.24	4.51	3.67	3.67	3.94	3.69	3.69	3.96	3.72	3.72	4.02
$Na(GaS_2)_2$	4.02	4.02	4.25	3.45	3.48	3.69	3.48	3.48	3.71	3.49	3.49	3.78
$K(GaS_2)_2$	3.85	3.85	4.07	3.27	3.27	3.50	3.29	3.29	3.50	3.47	3.47	3.60
$Cu(GaS_2)_2$	4.32	5.31	5.36	3.76	5.31	4.80	4.02	4.71	4.77	3.37	6.53	6.92
$Ag(GaS_2)_2$	4.25	5.41	5.42	3.67	5.41	4.86	3.84	4.94	4.83	3.27	5.60	5.64
$Au(GaS_2)_2$	4.25	5.35	5.36	3.71	5.35	4.80	3.87	4.76	4.78	3.46	4.07	5.27

Table 4: NBO charges on alkali and coinage metals in neutral and anionic clusters with the B3LYP functional[a]

Clusters	**NBO charges on alkali metals**		**Clusters**	**NBO charges on coinage metals**	
	Neutral	***Anion***		***Neutral***	***Anion***
$Li(GaO_2)_2$	0.45	0.87	$Cu(GaO_2)_2$	0.40	0.67
$Na(GaO_2)_2$	0.48	0.94	$Ag(GaO_2)_2$	0.41	0.77
$K(GaO_2)_2$	0.48	0.93	$Au(GaO_2)_2$	0.31	0.49
$Li(GaS_2)_2$	0.39	0.70	$Cu(GaS_2)_2$	0.28	0.38
$Na(GaS_2)_2$	0.44	0.83	$Ag(GaS_2)_2$	0.31	0.45
$K(GaS_2)_2$	0.46	0.86	$Au(GaS_2)_2$	0.15	0.25

[a] All values are in *e*.

Table 5: HOMO–LUMO gaps of the studied clusters with the B3LYP functional

Clusters	**HOMO–LUMO gaps**	**Clusters**	**HOMO–LUMO gaps**
$Li(GaO_2)_2$	5.04	$Li(GaS_2)_2$	4.74
$Na(GaO_2)_2$	4.79	$Na(GaS_2)_2$	4.37
$K(GaO_2)_2$	4.69	$K(GaS_2)_2$	4.36
$Cu(GaO_2)_2$	3.81	$Cu(GaS_2)_2$	3.99
$Ag(GaO_2)_2$	3.54	$Ag(GaS_2)_2$	3.33
$Au(GaO_2)_2$	3.41	$Au(GaS_2)_2$	4.10

Table 6: Dissociation energies (D_e, eV) of the studied clusters through different channels

Channels					**B3P86**	**B3PW91**	**B3LYP**	**MP2**
$Li(GaO_2)_2$	$\rightarrow$	$Li(GaO_2)$	+	GaO_2	3.99	3.92	3.71	4.64
$Li(GaO_2)_2$	$\rightarrow$	Li	+	$(GaO_2)_2$	5.09	4.88	4.98	5.48
$NaGaO_2)_2$	$\rightarrow$	$Na(GaO_2)$	+	GaO_2	4.06	3.98	3.79	4.69
$Na(GaO_2)_2$	$\rightarrow$	Na	+	$(GaO_2)_2$	4.26	4.07	4.09	4.74
$K(GaO_2)_2$	$\rightarrow$	$K(GaO_2)$	+	GaO_2	3.96	3.87	3.68	3.74
$K(GaO_2)_2$	$\rightarrow$	K	+	$(GaO_2)_2$	4.46	4.27	4.25	3.85
$Cu(GaO_2)_2$	$\rightarrow$	Cu	+	$(GaO_2)_2$	3.30	3.18	3.16	2.20
$Cu(GaO_2)_2$	$\rightarrow$	$Cu(GaO_2)$	+	GaO_2	3.99	3.91	3.71	4.45
$Ag(GaO_2)_2$	$\rightarrow$	Ag	+	$(GaO_2)_2$	2.60	2.47	2.44	2.15
$Ag(GaO_2)_2$	$\rightarrow$	$Ag(GaO_2)$	+	GaO_2	3.98	3.90	3.69	4.61
$Au(GaO_2)_2$	$\rightarrow$	Au	+	$(GaO_2)_2$	2.60	2.11	2.07	2.99
$Au(GaO_2)_2$	$\rightarrow$	$Au(GaO_2)$	+	GaO_2	4.40	4.32	4.08	4.80
$Li(GaS_2)_2$	$\rightarrow$	$Li(GaS_2)$	+	GaS_2	2.65	2.60	2.32	3.31
$Li(GaS_2)_2$	$\rightarrow$	Li	+	$(GaS_2)_2$	4.12	3.98	3.97	4.25
$Na(GaS_2)_2$	$\rightarrow$	$Na(GaS_2)$	+	GaS_2	2.47	2.41	2.23	3.08
$Na(GaS_2)_2$	$\rightarrow$	Na	+	$(GaS_2)_2$	3.55	3.41	3.34	3.74
$K(GaS_2)_2$	$\rightarrow$	$K(GaS_2)$	+	GaS_2	2.72	2.65	2.37	3.65
$K(GaS_2)_2$	$\rightarrow$	K	+	$(GaS_2)_2$	3.77	3.63	3.54	4.34
$CuGaS_2)_2$	$\rightarrow$	$Cu(GaS_2)$	+	GaS_2	2.86	2.76	2.48	2.19
$Cu(GaS_2)_2$	$\rightarrow$	Cu	+	$(GaS_2)_2$	3.49	3.34	3.21	3.60
$AgGaS_2)_2$	$\rightarrow$	$Ag(GaS_2)$	+	GaS_2	2.46	2.40	2.11	1.65
$Ag(GaS_2)_2$	$\rightarrow$	Ag	+	$(GaS_2)_2$	2.55	2.45	2.32	3.11
$Au(GaS_2)_2$	$\rightarrow$	Au	+	$(GaS_2)_2$	2.89	2.75	2.54	3.52
$AuGaS_2)_2$	$\rightarrow$	$Au(GaS_2)$	+	GaS_2	4.14	4.03	3.66	4.88

Table 7: Fragmentation energies (eV) with the DFT functionals

Functionals	**B3P86**	**B3PW91**	**B3LYP**
		$[K]^+[CuGa_2S_4]^-$	
ΔE_1	4.27	4.51	4.42
ΔE_2	3.54	3.97	3.82
ΔE_3	3.21	3.60	3.47
		$[K]^+[AgGa_2S_4]^-$	
ΔE_1	4.07	4.31	4.25
ΔE_2	3.41	3.71	3.55
ΔE_3	2.70	3.12	3.02
		$[K]^+[AuGa_2S_4]^-$	
ΔE_1	4.13	4.35	4.26
ΔE_2	3.51	3.75	3.61
ΔE_3	4.36	4.84	4.70

List of Figures

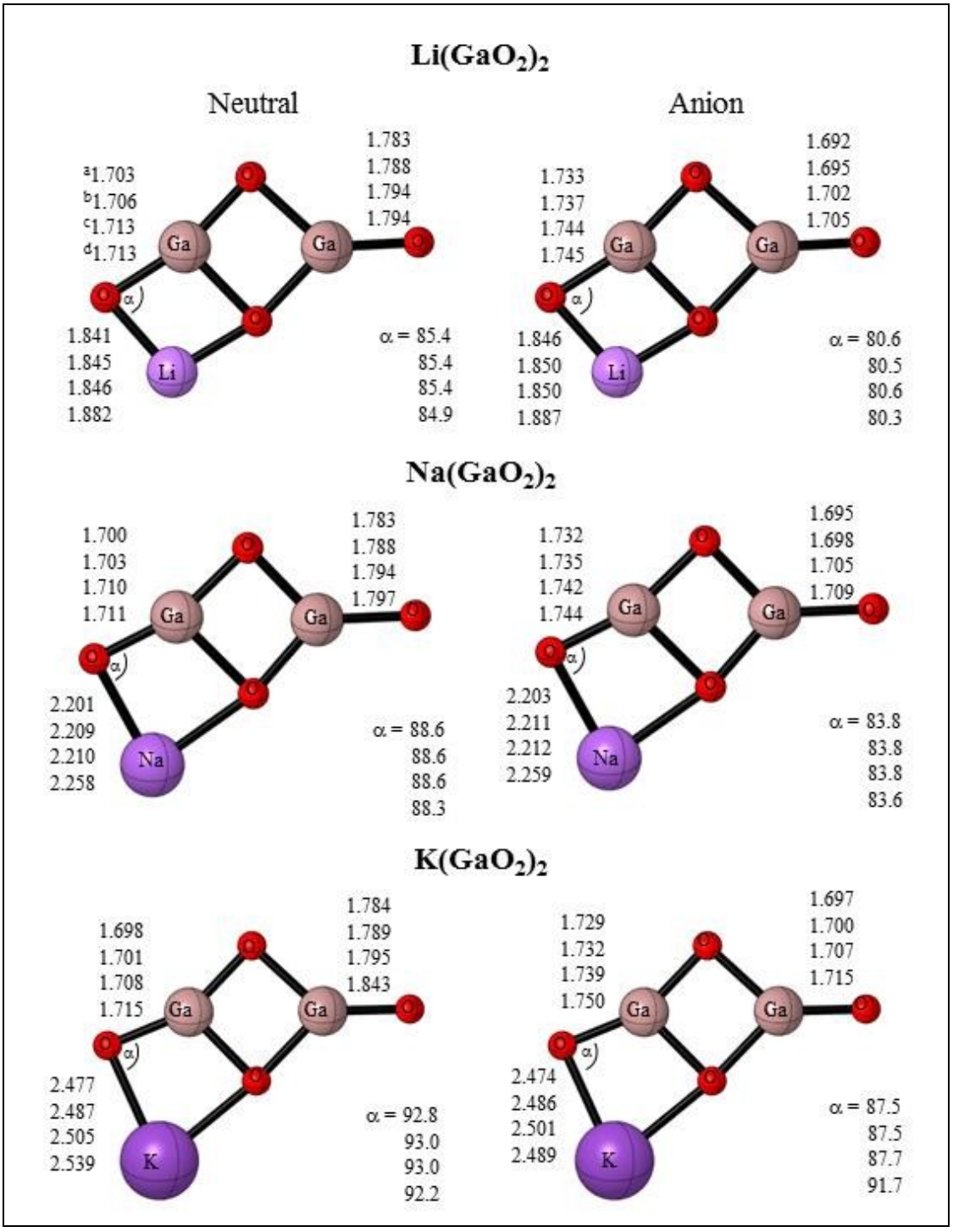

Fig. 1: Geometrical features of gallium oxide clusters containing alkali metals. Bond lengths are in Å and bond angles in °.

[a]B3P86, [b]B3PW91, [c]B3LYP and [d]MP2

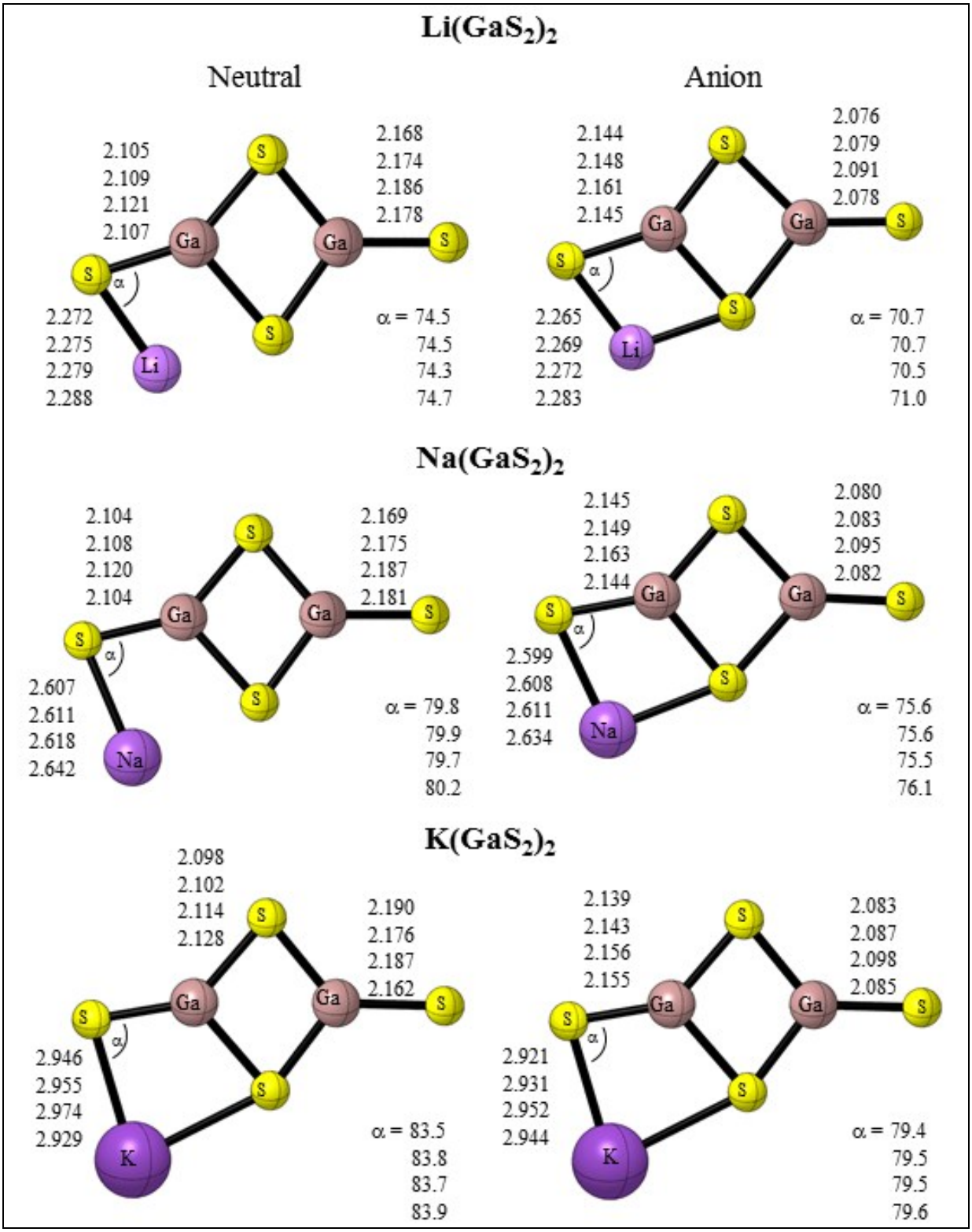

Fig. 2: Geometrical features of gallium sulfide clusters containing alkali metals.

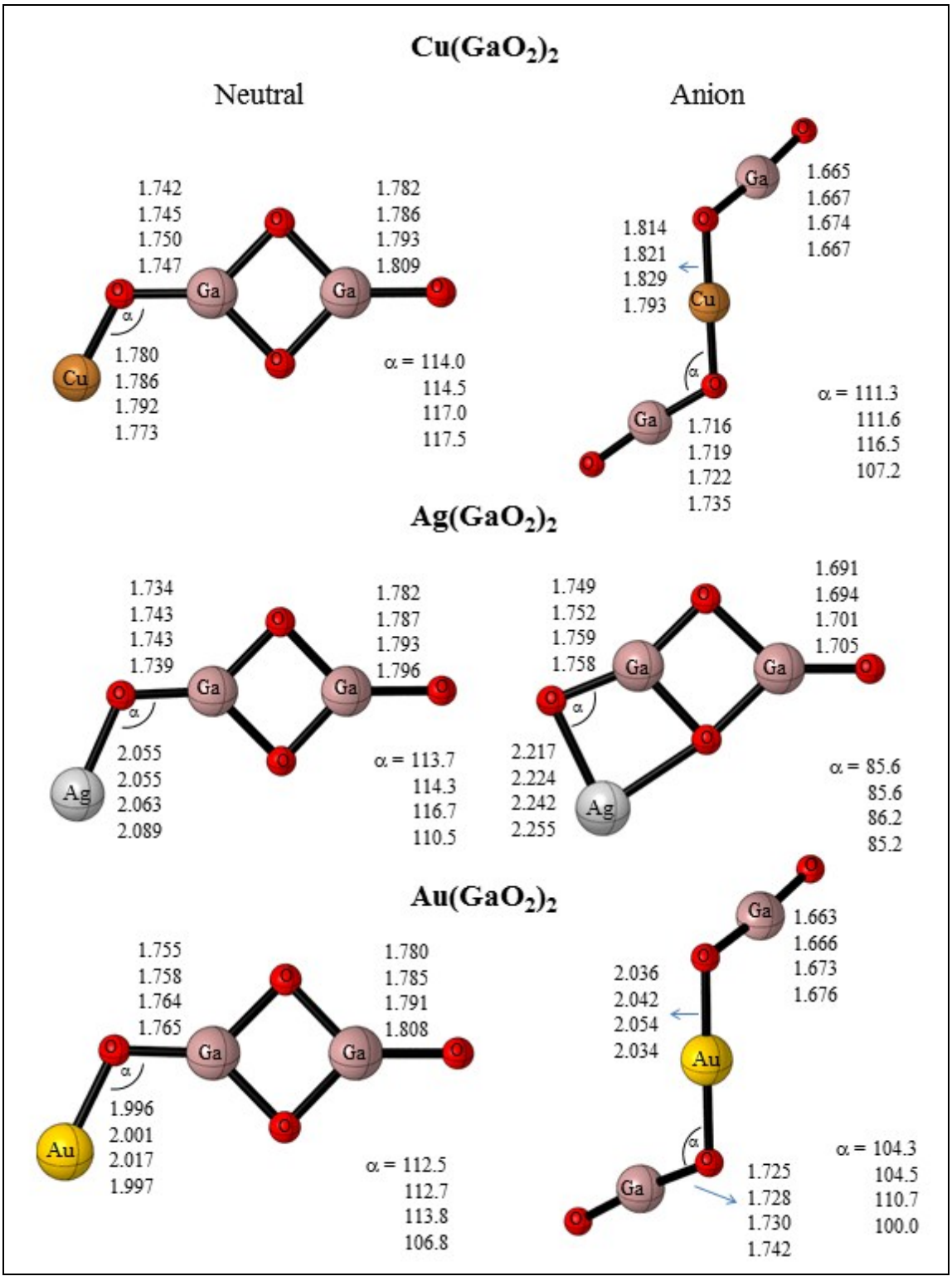

Fig. 3: Geometrical features of gallium oxide clusters containing coinage metals.

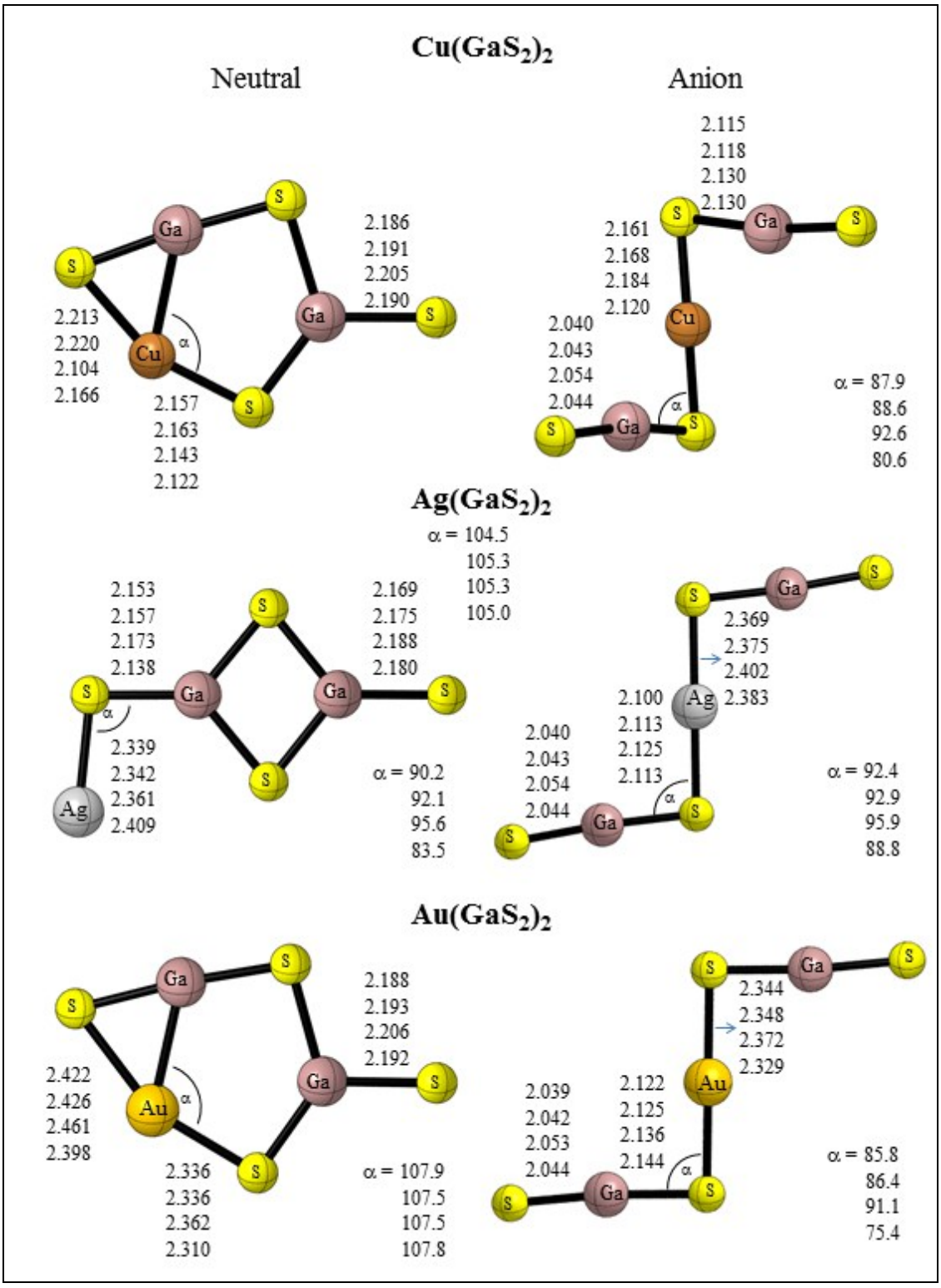

Fig. 4: Geometrical features of gallium sulfide clusters containing coinage metals.

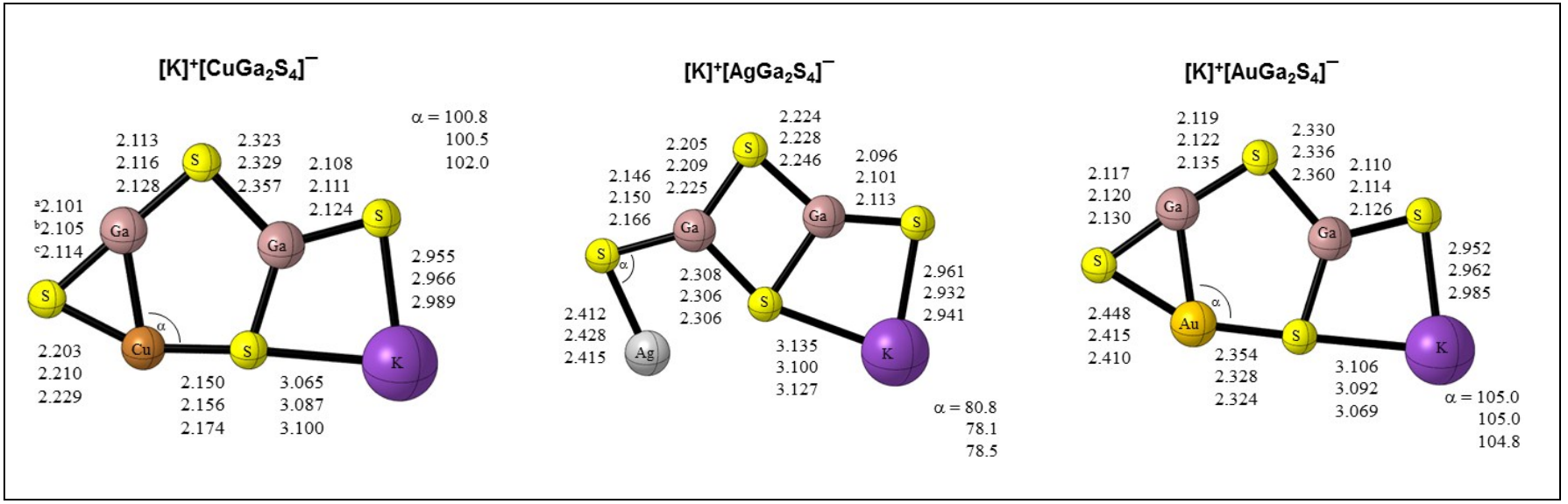

Fig. 5: Geometrical features of some proposed salts.

[a]B3P86, [b]B3PW91 and [c]B3LYP

Graphical Abstract